energy&fuels

pubs.acs.org/EF

Article

Novel Nuclear Magnetic Resonance Techniques To Assess the Wax Precipitation Evolution in Crude Oil Systems

G. C. Savulescu,* S. Simon, G. Sørland, and G. Øye

Cite This: *Energy Fuels* 2023, 37, 291−300

Read Online

ACCESS | Metrics & More | Article Recommendations | Supporting Information

ABSTRACT: Wax crystallization in cold environments constitutes one of the main causes for flow assurance problems during oil production. Several techniques, such as differential scanning calorimetry (DSC) or gas chromatography/mass spectroscopy (GC/MS), are currently the established methods for the quantification of wax precipitation. Low-field nuclear magnetic resonance (NMR) techniques have seldom been used for the investigation of wax precipitation, despite early studies showing their ability to identify the rate of precipitation. This paper highlights three NMR methods, adapted for the purpose of wax crystallization quantification in crude oil systems. The proposed methods are based on free induction decay (FID) and Carr−Purcell−Meiboom−Gill (CPMG) sequences. Both allow for the quantification of a signal that is proportional to the non-crystalline wax content, while FID data can also be used for the computation of the crystalline wax component in systems with a sufficiently high wax content. DSC is also used as a reference method for wax content quantification. Model system analysis demonstrates consistency between the three methods in toluene-based wax solutions and also highlights a thorough comparison between macro- and microcrystalline waxes. Similar results are obtained with the four methods for crude oils with a high wax content, and a relevant comparison between different systems can be achieved for oils with wax concentrations as low as 2% at 0 °C. Overall, the determination of the solid content with FID represents an improved, more reliable method, which can be utilized during the creation of more robust flow assurance methods.

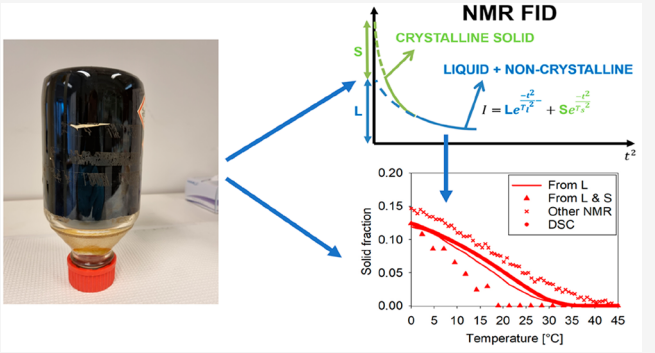

1. INTRODUCTION

Paraffin waxes are components of crude oil consisting of alkanes with variable chemical structures, normally with carbon chains between C_{20} and C_{100}.[1] Wax precipitation occurs in fluid environments at temperatures below the wax appearance temperature (WAT) and has negative effects on flow assurance during crude oil production. For example, the continuous flow might be interrupted by wax deposition and the resulting increase in fluid viscosity, while the restart of pipelines might be delayed by wax gelation.[2] Recently, the precipitation of waxes associated with the loss of gas and the gasoline fraction has been claimed to be involved in the unusual composition of some waxy crude oils.[3]

When the temperature is decreased, wax nucleation is delayed by a time lag required to overcome the shift from steady-state conditions. This delay depends upon the cooling rate,[4] and thus, the observed precipitation temperature with dynamic temperature ramping is usually lower than the actual precipitation temperature. Decreasing the cooling rate to very low values is the only way to overcome this effect.

During the last phase of crystallization, gelation is usually encountered in systems with wax contents above a threshold, which normally lies between 1 and 2%.[5] The gel can behave differently as a function of the chemical composition, particularly the isomerization of the waxes. For example, macrocrystalline wax, consisting of lower molecular weight *n*-alkanes, with up to 40 carbon atoms, is expected to generate gels with a high yield strength as a result of larger and less compact crystal structures. Oppositely, microcrystalline wax, composed of high-molecular-weight (C_{40} and above) iso-alkanes and cycloalkanes, leads to the formation of gels with a lower yield strength as a result of more compact crystal structures with smaller crystal diameters, with a higher percentage of amorphous structures.[6] Wax crystal formation might also be stimulated by introduction of surfaces or surfaces already present in crude oils, such as asphaltene aggregates.[7,8]

The evolution of wax precipitation with temperature has been quantified by following wax precipitation curves (WPCs) using techniques such as differential scanning calorimetry (DSC) and, more recently, low-field nuclear magnetic

Received: September 30, 2022
Revised: November 24, 2022
Published: December 13, 2022

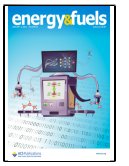

resonance (NMR).[9,10] Although DSC is an established method for calculations of the wax content, significant challenges remain when it comes to the analysis of crude oil systems. This can be mainly attributed to the complex chemical composition of crude oils that generates uncertainties in placing the baseline when estimating the latent enthalpies and heat capacities. Various approaches have been proposed to overcome these barriers;[9,11,12] however, none of them managed to eliminate these uncertainties completely.

NMR approaches have rarely been used to determine WPC in crude oil systems. Pedersen et al. were the first to introduce low-field NMR for the analysis of wax precipitation in crude oils.[13] They correlated the NMR signal intensity with the amount of wax generated by a modified acetone precipitation method performed at −20 °C for 17 crude oils. Later, the procedure has been significantly extended through the analysis of the NMR free induction decay (FID) signal,[14,15] but robust algorithms for calculation of the solid content from the NMR signal are still lacking.

In addition to the FID approach, an adapted Carr−Purcell−Meiboom−Gill (CPMG) sequence has been used to characterize model wax solutions in the presence of pour point depressants (PPDs) and asphaltenes.[16,10,17] Ruwoldt et al. compared the WPC generated with CPMG and DSC, respectively, and found that similar trends are achieved.[16] The most recent improvement was achieved by Savulescu et al., who adapted the CPMG sequence to wax precipitation curves in complex wax−asphaltene model systems.[10]

This study presents an improved NMR FID method combined with a novel algorithm for more accurate computations of the content of crystalline solids in crude oils. This resulted in higher resolution and less uncertainty of the wax precipitation curves compared to a standard computing algorithm used for FID data. Furthermore, wax precipitation curves were determined by NMR CPMG and DSC for comparison. Some weak points were identified for the latter method, and improvements were proposed.

2. EXPERIMENTAL SECTION

2.1. Materials. The solvents used in this study were deuterated toluene (anhydrous, 99.6% deuterated) and (hydrogenated) toluene (anhydrous, 99.8%) from Sigma-Aldrich, Norway. Macrocrystalline wax (coded 5405) and microcrystalline wax (coded 3971) were provided by Sasol, Germany. The composition and properties of the wax samples were presented previously.[16] Six crude oil samples from the Norwegian continental shelf were used. The densities of these oils at 30 °C and their elemental analysis are presented in Table 1. For crude oils 1−3, the elemental composition was determined by analysis at SGS France, while for crude oils 4−6, previously determined values were used.[18−20] For crude oils 1 and 3, the densities were measured with an Anton Paar DMA 5000 densiometer, while for crude oils 2 and 4−6, previously determined values were used.[18−20] All concentrations in this study are in weight percentages (wt %).

Table 1. Densities for Each Selected Crude Oil

crude oil	density (g/mL)	carbon content (%)	hydrogen content (%)	nitrogen content (%)	oxygen content (%)	sulfur content (%)
1	0.866	86.4	12.59	0.05	0.31	0.26
2	0.853	86.6	13.14	0.13	0.19	0.18
3	0.875	86.4	12.47	0.23	0.34	0.48
4	0.929	86.5	11.72	0.29	0.62	0.84
5	0.844	85.68	13.24	0.14	0.67	0.26
6	0.816	86.34	13.1	0.1	0.61	0.05

It can be noticed in Table 1 that the oxygen content is higher than the nitrogen and generally sulfur contents for the investigated oils. This observation can also be found for North Sea crude oils in the literature.[21]

2.2. Sample Preparation. Solid waxes were used as a reference in the NMR FID measurements. Wax solutions with varying concentrations (5−15%) were prepared by dissolution of wax in toluene or deuterated toluene. The systems containing macrocrystalline wax were heated at 60 °C for 1 h and shaken thoroughly. Because the systems containing microcrystalline wax have a higher WAT, they were heated at 80 °C for 1 h and shaken thoroughly. NMR FID and DSC measurements were carried out on these model wax systems. The crude oils were all heated at 80 °C and shaken thoroughly before the experiments. Crude oil 2 was also spiked with macrocrystalline wax and heated at 80 °C. NMR FID, NMR CPMG, and DSC measurements were carried out on these systems.

2.3. NMR Measurements. All NMR experiments were conducted on a low-field (21 MHz) NMR spectrometer, which was supplied by Anvendt Teknologi AS, Norway. The measurements were performed with 3 g of the respective samples in the NMR tubes. For the FID measurements, two independent parallels were performed for the model wax systems, while three independent parallels were performed for the crude oil systems, to ensure a higher degree of accuracy because these samples have variable, unknown chemical composition. For the CPMG measurements, two independent parallels were performed to ensure reproducibility. This method was primarily used on crude oils because its reliability for model systems has been investigated previously.[10]

2.3.1. NMR FID Analysis. The relaxation delay was measured 10 s after a 90° pulse width of 8.6 μs, and the signal was followed from 13 μs (the first point measurable with the NMR instrument) to 268 μs, at 1 μs intervals. The same acquisition was repeated 64 times. The average temperature ramping was fixed at 0.2 °C/min, which allowed for measurements at 19−20 temperature steps.

The FID analysis is based on the difference in relaxation speed for protons in a crystalline and non-crystalline phases. The total intensity of the signal plotted against the square of the acquired time is assumed to follow a bi-Gaussian equation

$$I \approx \mathbf{L}e^{-t^2/T_l^2} + \mathbf{S}e^{-t^2/T_s^2} \quad (1)$$

where **L** represents a parameter proportional to the amount of protons in the non-crystalline phase, T_l represents the modified FID relaxation time for the non-crystalline phase, **S** represents a parameter proportional to the amount of protons in the crystalline phase, T_s represents the modified FID relaxation time for the crystalline phase, and t is the acquisition time.[22−24] The modified relaxation time of the FID signal is limited by the T_2 relaxation time and can be correlated to it, following a relationship dependent upon the analyzed system.

For each temperature step, eq 1 was fitted to the first 80 points (i.e., from 13 to 92 μs) of the raw NMR signals using the *exp2* function in MATLAB 2021b. If the system was in the non-crystalline state or if a second exponential was not identifiable as a result of method limitations, a one-exponential fit was performed, using the *exp1* function in MATLAB 2021b. Extrapolation of the exponential functions to $t = 0$, illustrated in Figure 1, gave the signal proportional to the number of protons in the crystalline and non-crystalline phases, respectively, corresponding to **S** and **L** in eq 1. The R^2 values were consistently higher than 0.985 at 0 °C for both the two- and one-exponential fits.

Two approaches were used to calculate the fraction of solid-phase protons (f):

(1) "FID exponential separation" method: In this case, f is calculated by inserting the **L** and **S** values resulting from the biexponential fitting procedure above in the following equation:

$$f = \frac{\mathbf{S}}{\mathbf{S} + \mathbf{L}} \quad (2)$$

https://doi.org/10.1021/acs.energyfuels.2c03309
Energy Fuels 2023, 37, 291−300

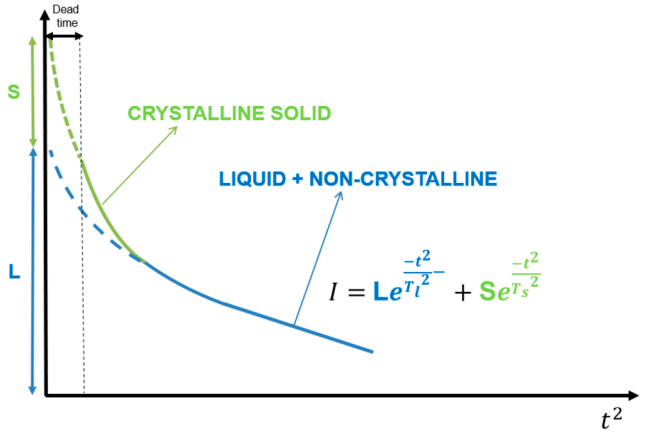

Figure 1. Schematic representation of the two-exponential separation for each NMR curve at a selected temperature (y axis) plotted as a function of the square of the acquisition time (x axis).

Two main challenges arise with this approach. One is accurate separation of the crystalline and non-crystalline regions. This is illustrated in Figure 2, showing the FID signal of pure macrocrystalline wax at 45 and 0 °C. At 0 °C, there is very little non-crystalline wax and there is a marked transition between the region with a low slope at long acquisition times, corresponding to non-crystalline wax, and the region with a high slope at short acquisition times, corresponding to crystalline wax. At 45 °C, on the other hand, the change from the non-crystalline to crystalline region is more gradual. This was attributed to the fact that the non-crystalline phase comprises parts with different mobilities. Higher mobility regions with lower slopes are noticed at higher acquisition times, while lower mobility regions with higher slopes are noticed at lower acquisition times. This results in larger errors for **L** and **S** when using the biexponential fitting. A higher number of exponentials could be theoretically used to separate states with different mobility, but this is not achievable with the results from low-field NMR, because the variation in modified relaxation time is not high enough.

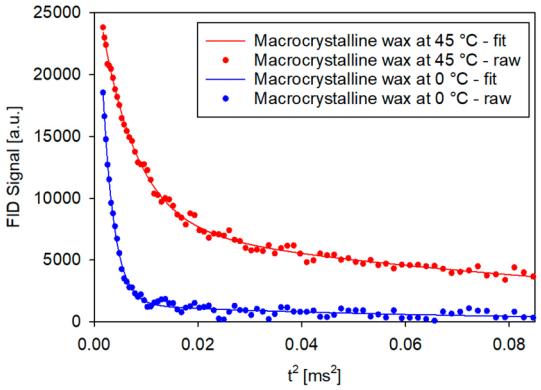

Figure 2. FID signal fitting with two exponentials for macrocrystalline wax at 45 and 0 °C.

The other main challenge with the approach is the dead time. This is illustrated in Figure 3, showing the FID signals and the corresponding two-exponential fits for crude oil 1 at 45 and at 0 °C. It is seen that the dead time limits the number of points obtained for the crystalline component in crude oil systems. Although there was a second exponential at low acquisition times when the temperature decreases to 0 °C, there were only about 7 points available for fitting this additional exponential. This decreased the certainty with which the extrapolated crystalline component was calculated. Crude oil 1 has the highest wax content among the analyzed oils, and thus, the degree of certainty for extrapolation decreases further for the rest of the oils.

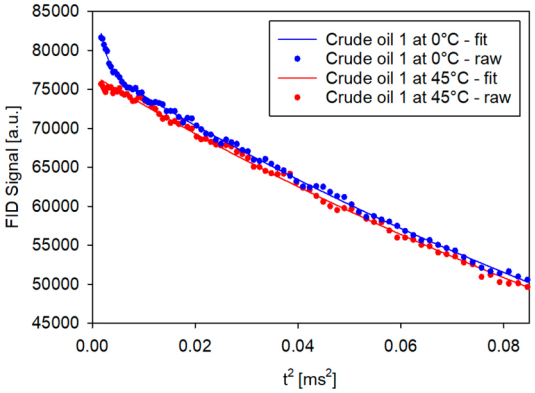

Figure 3. FID signal fitting at 0 °C for crude oil 1.

(2) "FID non-crystallized signal" method: This novel method is proposed in this work to avoid the above challenges when calculating the percentage of protons in the crystalline state. This approach focuses exclusively on the non-crystalline component **L**. Here, toluene was used as a reference to account for the signal change as a result of the variations in the repartition of energy of hydrogen atoms with the temperature.[25]

The drop in the fraction between the non-crystalline component in the system (L_T) and the non-crystalline component of toluene ($L_{\text{toluene},T}$) tracks the percentage of protons in the non-crystalline phase that is lost from the non-crystalline region as the temperature decreases from 45 °C to T. However, if the percentage of protons in the crystalline solid form (f) is higher than 0 at 45 °C (as for pure solid wax in Figure 2 for example), one should add the percentage of crystalline solid at 45 °C ($f_{45\ °C}$) because the normalized non-crystalline signal evolution only quantifies the drop from 45 °C onward. To find the crystalline solid value at 45 °C, the first proposed calculation method based on the two-exponential separation is used. The approach is summarized in the following equation for the fraction of protons in the crystalline solid state:

$$f = f_{45\ °C} + \frac{\frac{L_{45\ °C}}{L_{\text{toluene},45\ °C}} - \frac{L_T}{L_{\text{toluene},T}}}{\frac{L_{45\ °C}}{L_{\text{toluene},45\ °C}}} \quad (3)$$

A method presented by Kane et al.,[15] involving two assumptions, was used in both approaches to transform the fractions of crystalline solid protons into the weight fractions of the solid. The first assumption is that the density of the liquid remains constant during wax crystallization. To verify this, the density of macrocrystalline wax was extrapolated to be 0.792 g/mL from a curve with the inverse of the density plotted as a function of the mass fraction for different concentrations of wax (0, 1, 2.5, 5, 7.5, and 10%) in toluene. The crude oils had densities between 0.81 and 0.93 g/mL (Table 1). All of these densities are less than 20% higher than the estimated density of macrocrystalline wax, and because the maximum weight percentage of wax at 0 °C was found to be about 15% in the analyzed crude oils, it was considered that the actual density of the liquid in the crude oils would increase by a maximum of 3%, which is negligible. The second assumption is that the density and proton density of the precipitated solid are constant. This assumption might fail if asphaltenes or resins co-precipitate with the wax, because they have different proton densities and densities. In some cases, there might also be a significant difference between the density of the crude oil wax and the model wax used here. However, these parameters cannot be quantified, generating a limitation for this technique.

Two parallels were performed for the calibration with toluene, and both were independently used for solid fraction determination. For the analyzed systems, the f value for each parallel represents the average between the two solid fractions computed with each of the

https://doi.org/10.1021/acs.energyfuels.2c03309
Energy Fuels 2023, 37, 291−300

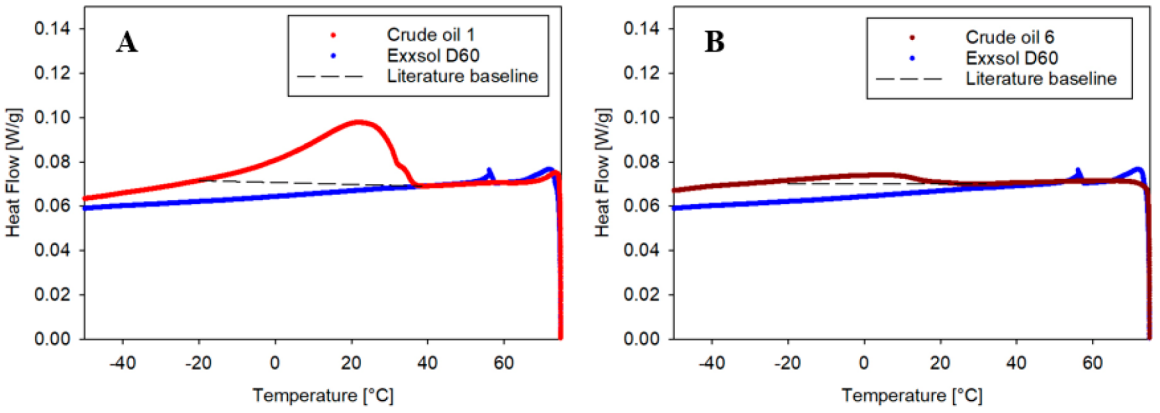

Figure 4. Baseline fitting using Exxsol D60, relative to baseline fitting using the method suggested by Chen et al. in the literature:[11] (A) crude oil 1 (high wax content) and (B) crude oil 6 (low wax content).

two parallels from toluene calibrations. The solid fraction presented in the graphs represents the average between the two or three parallels for each system of interest. For the solid fraction calculation process with FID, the following assumptions were made: constant density of the non-crystalline component of crude oil with the temperature and constant density equal to that of macrocrystalline wax 5405 from Sasol for the crystalline component in crude oils.

2.3.2. NMR CPMG Analysis. A CPMG sequence was used to acquire T_2 distributions,[26] following the procedure presented previously.[10] The recycle delay is 5 s, while the interecho spacing was selected for two regions. For the model systems, these sequence parameters were the same as presented previously.[10] For crude oil systems, on the other hand, they had to be adjusted, because the crude oils have a different distribution of the liquid T_2 region. In this case, there is a first region with τ_1 of 115 μs and 1000 echoes and a second region with τ_2 of 600 μs and 5000 echoes. These were selected to account for large signals in the long T_2 region in crude oil systems. T_2 distributions were generated from the multiexponentially decaying curve, using the one-dimensional inverse Laplace transform.[27] The intensity of T_2 represents a quantitative measure of the liquid signal with the temperature, which allows for the calculation of the lost solid content. Several algorithms in MATLAB 2021b were used to further process the data and separate the signal intensities in different T_2 areas, accordingly.

Stepwise temperature scanning was used from 45 to 0 °C, leaving the system at a constant temperature during signal acquisition at each temperature point. The ramping rate was 0.2 °C/min to ensure stable systems during the signal acquisition. The number of scans was set at a conventional value of 16, which allowed for measurements at 68 temperature steps.

The temperature inside the NMR was controlled with an air flow,[10] and calibration with hexadecane showed no thermal delay associated with the air flow. The average of two calibrations allowed to correct for the change in signal generated by the different repartitions of hydrogen atoms at different energy levels and quantified by the Boltzmann factor.[25] The wax content is calculated afterward using the procedures described previously.[16,10]

2.3.3. Choice of the NMR Sequences and the Intensity of the Magnetic Field. The chosen low-field NMR techniques, FID and CPMG, have significant differences that may impact the way results are acquired. The FID does not correct for magnetic field inhomogeneities, because it attenuates with a phase that is dependent upon fluctuations in the magnetic field experienced by the molecules. This is caused by either inhomogeneities in the external field or local fluctuations caused by the sample itself. In a solid, the local fluctuations are not changing significantly in time (long correlation time), while in a liquid, it is almost averaged out, i.e., fast diffusion limit. Thus, T_2 is much shorter in a solid than in a liquid, because the correlation time is much shorter in the liquid. Also, the external magnetic field inhomogeneities cause the liquid component to have a modified relaxation time, T_2*, of just a few milliseconds, while the true T_2 is of the order of seconds.

CPMG, on the other hand, does correct for external magnetic field inhomogeneities, and this affects the liquid component more than the solid component. For the solid component, the relaxation mechanism is more strongly coupled to the sample itself, because dipole−dipole coupling between molecules becomes important as a result of the long correlation time. This is the most important relaxation mechanism in the solid wax. The chosen method, however, only detects the liquid relaxation of the sample, which will be in this case determined by the true T_2 of the sample. Nonetheless, the noise in crude oil systems with complex chemical composition and proton species could reach high levels, and that is why this paper assesses whether CPMG or FID provides more accurate results with the selected instrument.

Low-field NMR was selected after initially assessing the potential of high-field NMR for the analysis of the desired systems. As an advantage, high-field NMR has a much better signal-to-noise ratio. However, as a result of chemical shifts, it is difficult to produce a CPMG decay properly with high-field NMR, and this prevents the accurate quantification of T_2 relaxation times. CPMG has real-time acquisition, and it will be the only component that is on resonance that will form spin echoes of a constant detection phase. Those molecules in a distance from the resonance frequency will be out of phase with a value dependent upon the interecho spacing, the τ value, and the chemical shift value. Thus, it can be completely out of phase with the spin echo on resonance, and this alters the CPMG acquisition. One could of course run spin echoes one by one and then analyze the spectrum each time, but this will be very time-consuming. In a low-field system, there is no chemical shift information available because the external field is weak and inhomogeneities prevent chemical shift resolution. Thus, it is much more unreliable to determine CPMG at high field using a superconducting magnet. Also, the sample size and price of the system favor the low-field instrumentation.

2.4. DSC. DSC measurements were carried out on a Q2000 model from TA Instruments. The instrument was calibrated by measuring the melting heat and temperature of pure indium. For each experiment, 10−25 mg of sample was weighed into Tzero hermetic aluminum pans and sealed hermetically. The weight of the pans was measured before and after the experiment to ensure that no solvent loss had occurred. Prior to the measurements, the samples were left isothermally at 80 °C for 10 min to ensure stabilization above the WAT. Initially, a constant cooling rate of 0.2 °C/min was used to keep the experimental conditions similar to the NMR experiments. However, it was impossible to set the baseline and identify the peak for several crude oils at such a low cooling rate because the curve flattened. Therefore, the experimental cooling rate was finally set to 2 °C/min. The temperature range was from 75 to −70 °C. Two parallels were performed for all systems.

https://doi.org/10.1021/acs.energyfuels.2c03309
Energy Fuels 2023, 37, 291−300

2.4.1. DSC Data Analysis. Determination of the baseline is essential for calculating the solid content from DSC measurements. Several challenges were encountered when applying different methods from the literature on crude oil systems. Pedersen et al. set the baseline as a straight line from the wax precipitation onset to the point where the heat flow curve flattens at low temperatures (down to −140 °C in their study), where all of the components of crude oil have stopped precipitating.[12] A drawback of this method is that the baseline is assumed to be a straight line, which is thermodynamically inaccurate. From a practical point of view, however, the instrument used in this study only allowed for measurements down to −70 °C, where the heat flow curves still declined. Coto et al.[9] introduced a baseline method based on fitting the liquid region of the heat flow curve at temperatures above the WAT and at temperatures below the end of crystallization into a second-order equation, dependent upon the temperature, following the model of the heat capacity for liquids. Improved models allowing for variations of latent heat with the molecular weight and using second-order equation fitting for the heat capacity were also suggested. Neither of these approaches were applicable for measurements where the heat flow did not flatten.

Chen et al.[11] set the baseline for crude oils as a straight line from the WAT to a temperature of −20 °C and calculated the wax content by correlating the enthalpy peak with the wax content in crude oil determined by a modified acetone precipitation method performed at −20 °C. This specific temperature is the temperature generally mentioned in the standard industrial method.[28] This approach is illustrated in Figure 4 for crude oils used in this study with high (A) and low (B) wax contents. The excess heat is clearly sensitive to the placement of the baseline, especially at low wax contents with less defined heat flows. Using this approach to calculate the wax content in the crude oils gave a loss in the peak as high as 70% compared to the NMR approaches because waxes were still precipitating at −20 °C.

A method using reference measurements of Exxsol D60 to set the baseline was therefore developed. Exxsol D60 was chosen as reference compound for several reasons: It is a mixture of alkanes and isoalkanes with a density similar to the density estimated for macrocrystalline wax (0.792 g/mL); the melting point is between −60 and −70 °C, which is well below the WAT; and the slope of the heat flow was similar to that for the crude oils studied here. Notably, these heat flow curves were modified by adding a constant term (Table S1 of the Supporting Information) to all data points, so that they would overlap with the heat flow curves for the various crude oils above the WAT. The resulting curves are shown in Figure 4 together with data for a crude oil with high (A) and low (B) wax contents. The excess peak was calculated by summing the heat flow from the wax precipitation onset to −20 °C, where all of the wax precipitated.[11] The percentage of the crystallized wax was then calculated as the ratio between the heat of the excess peak per gram and the standard latent heat of paraffin wax per gram. A value of 200 J/g was used for the latter,[29,30] which is an estimated value that might deviate in crude oils where the exact chemical composition is unknown. Furthermore, it was assumed that the specific crystallization heat did not change with the temperature (i.e., the excess heat and the mass of precipitated wax are constantly proportional).

3. RESULTS AND DISCUSSION

The presentation of results starts from selected model wax systems in air and toluene and progresses toward real, crude oil systems. The analysis is based on the comparison of wax precipitation curves from each of the four methods. Weaknesses and advantages of each technique were identified alongside the errors and inaccuracies as a result of assumptions.

3.1. Quantification of Solid Fractions in the Various Wax Systems. *3.1.1. Pure Waxes.* FID analysis of pure macro- and microcrystalline waxes was performed to verify the experimental approach and assess the two FID methods (eqs 2 and 3) for computing the solid fractions. Figure 5 presents the solid crystalline fractions of the pure macro- and microcrystalline waxes. The solid amounts are similar for both calculation methods, showing that both approaches were accurate for solids with uniform chemical composition. Furthermore, the amount of crystalline solid increased from 77 to 96% for macrocrystalline wax and from 52 to 83% for microcrystalline wax when the temperature decreased from 45 to 0 °C. Moreover, the higher amount of crystalline solid indicated a larger and stronger crystal structure for macrocrystalline wax, as explained in the Introduction. This has also been reported by others.[6]

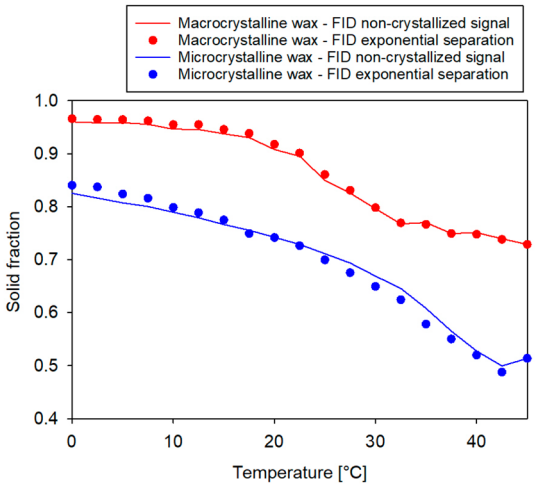

Figure 5. Solid fraction evolution with the temperature for pure wax systems, as calculated with the two proposed computation methods from FID data.

3.1.2. Wax in Toluene Systems. Figure 6 shows the solid crystalline fraction determined by the various techniques for 15% macrocrystalline wax in hydrogenated toluene. An overall trend of increasing solid fractions with decreasing temperature was observed in all cases. However, differences between the experimental techniques and between the FID computing methods emerged. In comparison of the experimental techniques, the wax precipitation curves were similar for the CPMG and DSC measurements and the onset of wax precipitation was detected at a lower temperature compared to the FID measurements. This difference could be explained by the higher cooling rate for DSC,[4,31,32] but because the

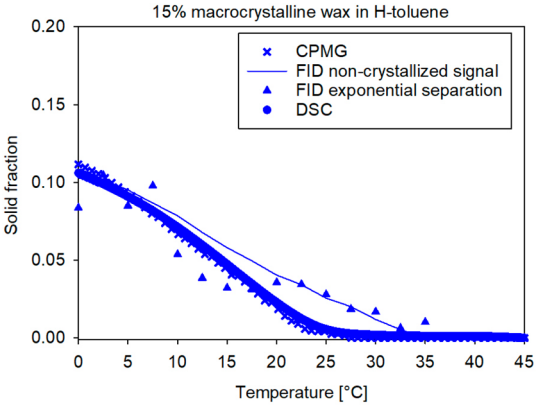

Figure 6. Solid fraction evolution with the temperature for 15% macrocrystalline wax in hydrogenated toluene, with all proposed methods. For CPMG, the value obtained by Savulescu et al.[10] is used.

https://doi.org/10.1021/acs.energyfuels.2c03309
Energy Fuels 2023, 37, 291−300

cooling rate was the same in the CPMG and FID measurements, another factor is most likely dominating. Hence, the presence of amorphous phases in the lower mobility part of the non-crystalline region, specific to the nature of dissolved wax in each system, may affect the exponential separation process and may be accounted for as crystalline solid, leading to an overestimation of the crystalline content at the first stage of crystallization. Nonetheless, between 25 and 35 °C, the wax content determined with FID remains within the maximum absolute error of the method (approximately 2−3%). As temperature decreases, most of these phases are likely to change into crystalline wax, and as the solid exponential becomes stronger, the uncertainty for FID decreases and the gap between FID and CPMG/DSC reduces. In comparison of the two calculation approaches for the FID measurements, the "FID non-crystallized signal" method gave a quasi-linear wax precipitation curve that converged with the DSC and CPMG curves at low temperatures. The "FID exponential separation" method, on the other hand, gave a less even and more disordered curve. This can be associated with the increased signal from the non-crystalline region when going from pure waxes to waxes in hydrogenated toluene, because at least 85% of the mass will generate a signal in this region. The solid exponential thus becomes more difficult to separate and is more likely to extend into the dead time.

To assess the accuracy of the NMR FID approach, wax precipitation was compared for 15% macro- and microcrystalline waxes in both hydrogenated toluene (Figure S1 of the Supporting Information) and deuterated toluene (Figure S2 of the Supporting Information). In the latter solvent, the entire NMR signal was due to the wax and improved the determination of the solid fractions.

The sensitivity of the NMR FID approach was assessed by following the precipitation of solid wax for 5, 10, and 15% wax solutions (Figure S3 of the Supporting Information). A crystalline solid component could be determined at 15 and 10% wax but no longer at 5% wax for the "FID non-crystallized signal" method. This was probably due to a shift of the crystalline solid decay into the dead time as the wax content decreased (Figure S4 of the Supporting Information), making quantification impossible.

3.1.3. Crude Oils with a High Wax Content. Only crude oil 1 had a sufficiently high wax content to be detected at low temperatures by all of the approaches. The wax precipitation curves are shown in Figure 7 and are similar for the DSC and NMR FID measurements using the "FID non-crystallized signal" method, while the CPMG measurements gave a somewhat higher solid content in the entire temperature range. An explanation for this can be that the CPMG signal is only detected in the liquid region defined by a fixed T_2 range (10^{-3}−10^{1} s), while the entire liquid and solid signals are detected in the FID method. Thus, the CPMG approach will count both liquid and solid phases outside the T_2 range as solid, while only the solid fraction will account for the FID non-crystallized method. The FID exponential separation method, on the other hand, gave a lower onset temperature for the wax precipitation and generally lower amounts of solids, even though the difference from the other methods decreased as the temperature approached 0 °C, as a result of difficulties in separating two exponentials at the first few temperatures after the onset of crystallization and the presence of amorphous phases during ongoing precipitation, which alter the exponential separation process. Moreover, the detection limit for the method was 2−3% solid for crude oil 1, which is in accordance with what was observed in the model systems.

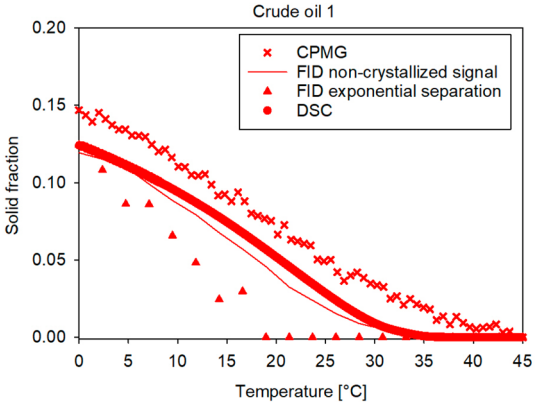

Figure 7. Solid fraction evolution with the temperature for crude oil 1, with all proposed methods.

To study the influence of chemical composition, 15% macrocrystalline wax was dissolved in crude oil 2. The amounts detected by the various methods at a given temperature were different from both crude oils 1 and 2 enriched with wax (Figure S5 of the Supporting Information). Furthermore, the detection limit for the FID exponential separation method was 6−7% solid in this case. This can be attributed to the difference in the chemical composition because the detected amounts might be dependent upon the nature of the wax crystals, specific to each system.

The presented methods and procedures cannot separate between macro- and microcrystalline wax. NMR FID/CPMG focuses on separating crystalline and non-crystalline phases in the crude oil. It is currently not possible to quantify the proportion of macro- and microcrystalline wax molecules in the crystallized phase.

3.1.4. Crude Oils with a Low Wax Content. The wax precipitation curves for the crude oils with a low (<10%) wax content are presented in Figure 8 for crude oil 3 and Figures S6, S7, S8, and S9 of the Supporting Information for crude oils 2, 4, 5, and 6, respectively. For these samples, it was not possible to separate two exponentials in the FID signal; therefore, no solid fractions were calculated with the FID exponential separation method. Furthermore, a low signal-to-noise ratio for CPMG measurements prevented calculations of

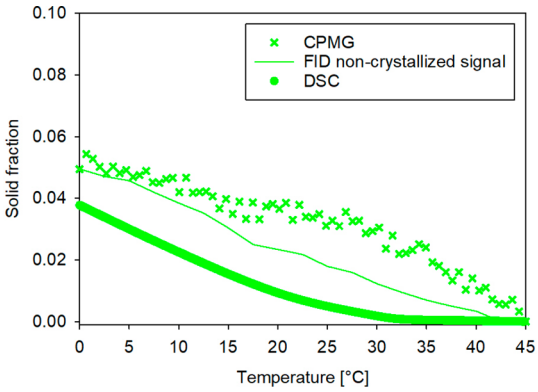

Figure 8. Solid fraction evolution with the temperature for crude oil 3, with all proposed methods.

https://doi.org/10.1021/acs.energyfuels.2c03309
Energy Fuels 2023, 37, 291−300

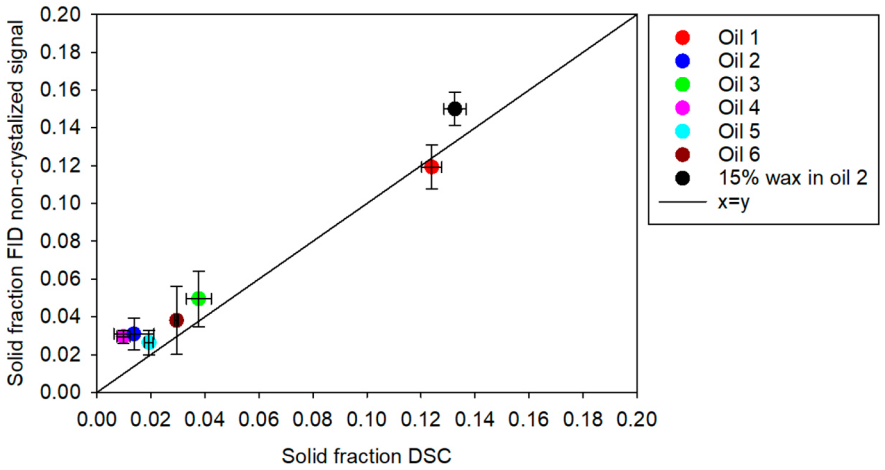

Figure 9. Solid fraction with the FID non-crystallized signal calculation technique as a function of the solid fraction with DSC at 0 °C.

Table 2. Average Errors during Reproducibility at 0 °C with NMR FID, NMR CPMG, and DSC for Model and Real Systems[a]

system	CPMG (wt %)	DSC (wt %)	FID exponential separation (wt %)	FID non-crystallized signal (wt %)
crude oil 1	14.68 ± 0.39	12.40 ± 0.37	12.41 ± 0.18	11.78 ± 1.18 (1.36)
crude oil 2	ND	1.37 ± 0.74	ND	3.09 ± 0.83 (2.19)
crude oil 3	4.94 ± 0.05	3.77 ± 0.46	ND	5.67 ± 1.47 (1.66)
crude oil 4	ND	0.98 ± 0.25	ND	2.95 ± 0.34 (1.46)
crude oil 5	3.52 ± 0.50	1.93 ± 0.16	ND	2.64 ± 0.64 (1.95)
crude oil 6	4.28 ± 0.40	2.95 ± 0.06	ND	3.81 ± 1.80 (3.20)

[a]ND = not detectable. The error bars represent the range of obtained values.

solid fractions for two of the samples (crude oils 2 and 4 in Figures S6 and S7 of the Supporting Information, respectively). In addition, it seems that the solid fraction did not plateau at 0 at the highest temperatures for crude oil 3 (Figure 8) as a result of the very low wax content in this crude oil associated with the uncertainties from instrumental noise issues.

Generally, the CPMG measurements gave solid fractions somewhat higher than for the other methods. However, the onset of wax precipitation and a quasi-linear precipitation pattern are similar to the FID non-crystallized signal method. The DSC measurements, on the other hand, give a lower precipitation onset temperature with an accelerating precipitation rate below 15 °C and lower solid fractions over the investigated temperature for all of the crude oil samples. The causes behind this can be higher cooling rates resulting in delayed precipitation and assumptions about constant heat capacity and proportionality between the amount of heat and the mass of solid, which might not be valid for wax systems with complex chemical composition, where the various latent heat and molecular mass profiles might differ in different regions.[29,30] Moreover, the wax content is sensitive to the baseline, as explained above. It should also be noted that uncertainties in each of the methods can give overlapping results. This is discussed further in the next section.

3.2. Evaluation of the Investigated Techniques. Figure 9 presents a comparison between the solid fraction determined with the FID non-crystallized signal method and DSC for crude oil systems at 0 °C. In most cases, the FID non-crystallized signal method gives somewhat higher wax contents than DSC, likely as a result of the assumptions and differences in the cooling rate discussed above and increases in relative values as the wax content in the oil decreases.

Table 2 shows the solid contents with errors at 0 °C determined for the crude oils by the various techniques. In all cases, the errors between two or three parallels are given, calculated using the average toluene calibration values for the FID non-crystallized signal method. For the latter approach, the error between the four parallels performed for toluene calibration was also considered. These errors are given in parentheses and correspond to the highest possible errors because the most and least favorable parallels were used for both the sample and calibration measurements.

The FID exponential separation method was not applicable for low wax content samples because a minimum solid content of about 2% is needed to distinguish two exponentials in the FID decay.

Determination of low wax contents was also challenging using the CPMG approach, mainly because of instrument noise. Furthermore, a high degree of noise resulted in considerable variations in the solid content from one temperature to another in several circumstances.

This left DSC and the FID non-crystallized method as the two approaches for determining a broad range of wax contents. DSC gave the lowest error (a maximum of 0.74 percentage points) but also included thermodynamic assumptions, assumption of similar chemical composition of the wax for all of the samples, and baseline determination using Exxsol D60 data. The FID non-crystallized signal method, on the other hand, is based on assumptions mainly related to exponential separation and signal-to-noise issues generated by the NMR instrument. Considering the error between parallels, the maximum error was seen at 1.8% for crude oil 6.

With the variation between parallels for the calibration with toluene taken into account, the error increased up to 3.2%. This is generated by the uncertainty in the ratio of the toluene

https://doi.org/10.1021/acs.energyfuels.2c03309
Energy Fuels 2023, 37, 291−300

liquid component at 45 °C and the toluene liquid component at 0 °C. For the four parallels performed for toluene, this ratio was within a 5% error for three cases and deviated up to 15% upward for one case, which causes a significant deviation when used to assess error. However, this error will cause the same effect on the computed solid fraction for all systems of interest. If the FID non-crystallized signal method is routinely used to characterize the wax content in crude oils, the accuracy should most likely be improved, especially for a low wax content. The uncertainties in the FID can be reduced by improving the signal-to-noise ratio, increasing the number of parallels, and advancement in instrumental accuracy.

The FID-based methods for computation of solid fractions can also be discussed in view of methods reported in the literature. A NMR FID method was, for example, standardized to calculate the solid fat content in various systems.[33,34] In this case, the non-crystalline and crystalline contents were separated as linear fractions (rather than using two- or one-exponential models), while a calibration factor, calculated using solid-containing standard samples, was used to account for the dead time.[15,35] This fails to account for the nature of the FID signal[24] and also generated a high degree of error because a linear fit cannot be applied at fixed time points.

Declerck et al. showed that this method was only suitable for fats with a certain chemical composition. In rapeseed and sunflower oils, for example, fats containing mostly α-polymorphs generated good results, while fats based on $\beta(')$ crystals, where the signal decay depended upon the crystal lattice and polymorphism, generated inappropriate results. Better results were obtained using the bi-Gaussian FID approach to calculate the solid fractions.[22]

Several improvements of these approaches were considered in the current work, where samples with solid contents too low for a solid exponential to be detected were often encountered. Hence, a one-exponential alternative normalized with toluene was proposed. Another drawback was that the liquid exponential was calculated only for the FID signal values longer than 50 μs, which is inaccurate for the identification of the crystalline content in crude oils. In the approach presented in this article, the exponentials are fitted on the first 80 points and the abrupt change in T_2 behavior between crystalline and non-crystalline components was the basis of exponential separation. The ratio between the liquid- and solid-modified relaxation times is consistently high, between 4 and 20 (Table S2 of the Supporting Information), confirming the abrupt change in exponent when the crystalline content starts forming, which further solidifies the use of the two-exponential fit. Separating the liquid from 50 μs would mean that the calculated solid fraction would comprise both crystalline and amorphous solid−liquid transition phases, which are non-crystalline and should not account for the crystalline solid fraction. Moreover, the selection of a specific border point at 50 μs represents an additional assumption.

4. CONCLUSION

This work highlights a novel approach to characterize the crystalline wax content in crude oils based on low-field NMR, which represents an addition and an improvement to established procedures based on DSC, because it allows for the quantification of the solid content at a very low cooling rate, without thermodynamic and baseline determination assumptions. The main novelty in this study is the development of a suitable exponential fit for the FID signal, followed by its application to compute the crystalline solid content in crude oils. The method starts from assessing the crystalline solid fraction in model systems with a high content, resembling at this step the procedures previously applied for solid fat calculation. Thus, the NMR methods were all validated for model systems. However, the content of solid states in crude oil is significantly lower than that in fats and pure waxes, particularly in the temperature range of interest for assessing dynamic wax crystallization. Therefore, the exponential-based model was adapted for such systems, and the method of calculation was split into two cases: the first where the crystalline and non-crystalline components were entirely separated and assessed and the second where the non-crystalline component was evaluated relative to a pure liquid. This second approach allows for the assessment of the solid content, starting from early stages of wax crystallization, while the first FID method is only applicable when the crystallized solid content is high enough (a few percentages). There are, however, some limitations generated by the instrument dead time, inability to separate amorphous phases completely, and chemical composition assumptions about the wax in crude oil. Nevertheless, these barriers can be overcome as NMR instruments become more advanced, by lowering the noise and dead times. Moreover, the direct comparison of results and calculation methods with DSC and NMR CPMG confirms the quality of the method and even indicates higher reliability and lower sensitivity on assumptions with the non-crystallized signal FID method. This creates the groundwork for an improvement in wax crystallization studies using NMR as an alternative to established methods.

■ ASSOCIATED CONTENT

Supporting Information

The Supporting Information is available free of charge at https://pubs.acs.org/doi/10.1021/acs.energyfuels.2c03309.

Normalization of the DSC curves of crude oils to fit Exxsol D60 in the high-temperature region (Table S1), solid fraction calculated with the two FID methods for macro- and microcrystalline wax in both hydrogenated (Figure S1) and deuterated (Figure S2) toluene, comparison between macrocrystalline wax solutions with varying concentrations in toluene to assess the impact of the wax concentration on the accuracy of the method (Figures S3 and S4), solid fraction as calculated with all of the available methods for 15% macrocrystalline wax in crude oil 2 and crude oils 2, 4, 5, and 6 (Figures S5, S6, S7, S8, and S9), respectively, and indication of the crystalline and non-crystalline average exponential times computed in the biexponential fit (Table S2) (PDF)

■ AUTHOR INFORMATION

Corresponding Author

G. C. Savulescu − *Ugelstad Laboratory, Department of Chemical Engineering, Norwegian University of Sciences and Technology (NTNU), N-7491 Trondheim, Norway;* orcid.org/0000-0003-3278-0745; Phone: +4798655325; Email: george.c.savulescu@ntnu.no

https://doi.org/10.1021/acs.energyfuels.2c03309
Energy Fuels 2023, 37, 291−300

Authors

S. Simon − *Ugelstad Laboratory, Department of Chemical Engineering, Norwegian University of Sciences and Technology (NTNU), N-7491 Trondheim, Norway*

G. Sørland − *Ugelstad Laboratory, Department of Chemical Engineering, Norwegian University of Sciences and Technology (NTNU), N-7491 Trondheim, Norway; Anvendt Teknologi AS, N-7022 Trondheim, Norway*

G. Øye − *Ugelstad Laboratory, Department of Chemical Engineering, Norwegian University of Sciences and Technology (NTNU), N-7491 Trondheim, Norway*

Complete contact information is available at: https://pubs.acs.org/10.1021/acs.energyfuels.2c03309

Notes

The authors declare no competing financial interest.

■ ACKNOWLEDGMENTS

This work is part of SUBPRO SFI, a research-based center within subsea production and processing. The authors hereby acknowledge the financial support from SUBPRO, which is financed by the Research Council of Norway, major industry partners, and NTNU.

■ REFERENCES

(1) Oliveira, L. M. S. L.; Nunes, R. C. P.; Melo, I. C.; Ribeiro, Y. L. L.; Reis, L. G.; Dias, J. C. M.; Guimarães, R. C. L.; Lucas, E. F. Evaluation of the Correlation between Wax Type and Structure/Behavior of the Pour Point Depressant. *Fuel Process. Technol.* **2016**, *149*, 268−274.

(2) Kelland, M.*Production Chemicals for the Oil and Gas Industry*; CRC Press: Boca Raton, FL, 2009; Vol. *1*, DOI: 10.1201/9781420092974.

(3) Gan, Y.; Chen, L.; Zhang, J.; Betancourt, S. S.; Mullins, O. C.; Yan, Z.; Gao, X.; Tian, J.; Chen, W.; Wang, W. Wax-Out Cryo-Trapping: A New Trap-Filling Process in Fluid Migration to Oilfields. *Energy Fuels* **2022**, *36* (16), 8844−8852.

(4) Paso, K.; Senra, M.; Yi, Y.; Sastry, A. M.; Fogler, H. S. Paraffin Polydispersity Facilitates Mechanical Gelation. *Ind. Eng. Chem. Res.* **2005**, *44* (18), 7242−7254.

(5) Venkatesan, R.; Nagarajan, N. R.; Paso, K.; Yi, Y.-B.; Sastry, A. M.; Fogler, H. S. The Strength of Paraffin Gels Formed under Static and Flow Conditions. *Chem. Eng. Sci.* **2005**, *60* (13), 3587−3598.

(6) Yang, F.; Zhao, Y.; Sjoblom, J.; Li, C.; Paso, K. G. Polymeric Wax Inhibitors and Pour Point Depressants for Waxy Crude Oils: A Critical Review. *J. Dispersion Sci. Technol.* **2015**, *36* (2), 213−225.

(7) Kriz, P.; Andersen, S. I. Effect of Asphaltenes on Crude Oil Wax Crystallization. *Energy Fuels* **2005**, *19* (3), 948−953.

(8) Norrman, J.; Solberg, A.; Sjöblom, J.; Paso, K. Nanoparticles for Waxy Crudes: Effect of Polymer Coverage and the Effect on Wax Crystallization. *Energy Fuels* **2016**, *30* (6), 5108−5114.

(9) Coto, B.; Martos, C.; Espada, J. J.; Robustillo, M. D.; Peña, J. L. Analysis of Paraffin Precipitation from Petroleum Mixtures by Means of DSC: Iterative Procedure Considering Solid−Liquid Equilibrium Equations. *Fuel* **2010**, *89* (5), 1087−1094.

(10) Savulescu, G. C.; Simon, S.; Sørland, G.; Øye, G. New Nuclear Magnetic Resonance Approaches on the Evolution of Wax Mobility during Wax Crystallization. *Energy Fuels* **2022**, *36* (1), 350−360.

(11) Chen, J.; Zhang, J.; Li, H. Determining the Wax Content of Crude Oils by Using Differential Scanning Calorimetry. *Thermochim. Acta* **2004**, *410* (1−2), 23−26.

(12) Baltzer Hansen, A.; Larsen, E.; Batsberg Pedersen, W.; Nielsen, A. B.; Roenningsen, H. P. Wax Precipitation from North Sea Crude Oils. 3. Precipitation and Dissolution of Wax Studied by Differential Scanning Calorimetry. *Energy Fuels* **1991**, *5* (6), 914−923.

(13) Batsberg Pedersen, W.; Baltzer Hansen, A.; Larsen, E.; Nielsen, A. B.; Roenningsen, H. P. Wax Precipitation from North Sea Crude Oils. 2. Solid-Phase Content as Function of Temperature Determined by Pulsed NMR. *Energy Fuels* **1991**, *5* (6), 908−913.

(14) Ruffier-Meray, V.; Roussel, J.; Defontaines, A. Use of Pulsed NMR Spectroscopy to Measure the Amount of Solid Deposits as a Function of Temperature in Waxy Crudes. *Oil Gas Sci. Technol.* **1998**, *53*, 531−535.

(15) Kané, M.; Djabourov, M.; Volle, J.-L.; Rutledge, D. N. Correction of Biased Time Domain NMR Estimates of the Solid Content of Partially Crystallized Systems. *Appl. Magn. Reson.* **2002**, *22* (3), 335−346.

(16) Ruwoldt, J.; Humborstad Sørland, G.; Simon, S.; Oschmann, H.-J.; Sjöblom, J. Inhibitor-Wax Interactions and PPD Effect on Wax Crystallization: New Approaches for GC/MS and NMR, and Comparison with DSC, CPM, and Rheometry. *J. Pet. Sci. Eng.* **2019**, *177*, 53−68.

(17) Zhao, Y.; Paso, K.; Norrman, J.; Ali, H.; Sørland, G.; Sjöblom, J. Utilization of DSC, NIR, and NMR for Wax Appearance Temperature and Chemical Additive Performance Characterization. *J. Therm. Anal. Calorim.* **2015**, *120* (2), 1427−1433.

(18) Dudek, M.; Kancir, E.; Øye, G. Influence of the Crude Oil and Water Compositions on the Quality of Synthetic Produced Water. *Energy Fuels* **2017**, *31* (4), 3708−3716.

(19) Dudek, M.; Bertheussen, A.; Dumaire, T.; Øye, G. Microfluidic Tools for Studying Coalescence of Crude Oil Droplets in Produced Water. *Chem. Eng. Sci.* **2018**, *191*, 448−458.

(20) Simon, S.; Nenningsland, A. L.; Herschbach, E.; Sjöblom, J. Extraction of Basic Components from Petroleum Crude Oil. *Energy Fuels* **2010**, *24* (2), 1043−1050.

(21) Gaweł, B.; Eftekhardadkhah, M.; Øye, G. Elemental Composition and Fourier Transform Infrared Spectroscopy Analysis of Crude Oils and Their Fractions. *Energy Fuels* **2014**, *28* (2), 997−1003.

(22) Declerck, A.; Nelis, V.; Rimaux, T.; Dewettinck, K.; Van der Meeren, P. Influence of Polymorphism on the Solid Fat Content Determined by FID Deconvolution. *Eur. J. Lipid Sci. Technol.* **2018**, *120* (3), 1700339.

(23) Abragam, A.*Principles of Nuclear Magnetism*; Oxford University Press: Oxford, U.K., 1961.

(24) Trezza, E.; Haiduc, A. M.; Goudappel, G. J. W.; van Duynhoven, J. P. M. Rapid Phase-Compositional Assessment of Lipid-Based Food Products by Time Domain NMR. *Magn. Reson. Chem.* **2006**, *44* (11), 1023−1030.

(25) Slichter, C. P.*Principles of Magnetic Resonance*; Springer-Verlag: Berlin, Germany, 2013.

(26) Meiboom, S.; Gill, D. Modified Spin-Echo Method for Measuring Nuclear Relaxation Times. *Rev. Sci. Instrum.* **1958**, *29* (8), 688−691.

(27) Provencher, S. W. A Constrained Regularization Method for Inverting Data Represented by Linear Algebraic or Integral Equations. *Comput. Phys. Commun.* **1982**, *27* (3), 213−227.

(28) Burger, E. D.; Perkins, T. K.; Striegler, J. H. Studies of Wax Deposition in the Trans Alaska Pipeline. *J. Pet. Technol.* **1981**, *33* (6), 1075−1086.

(29) Agarwal, A.; Sarviya, R. M. Characterization of Commercial Grade Paraffin Wax as Latent Heat Storage Material for Solar Dryers. *Mater. Today Proc.* **2017**, *4* (2, Part A), 779−789.

(30) Mochane, M. J.; Mokhena, T. C.; Motaung, T. E.; Linganiso, L. Z. Shape-Stabilized Phase Change Materials of Polyolefin/Wax Blends and Their Composites. *J. Therm. Anal. Calorim.* **2020**, *139* (5), 2951−2963.

(31) Japper-Jaafar, A.; Bhaskoro, P. T.; Mior, Z. S. A New Perspective on the Measurements of Wax Appearance Temperature: Comparison between DSC, Thermomicroscopy and Rheometry and the Cooling Rate Effects. *J. Pet. Sci. Eng.* **2016**, *147*, 672−681.

(32) Ruwoldt, J.; Kurniawan, M.; Oschmann, H.-J. Non-Linear Dependency of Wax Appearance Temperature on Cooling Rate. *J. Pet. Sci. Eng.* **2018**, *165*, 114−126.

(33) Dieffenbacher, A.; Pocklington, W. D.*Standard Methods for the Analysis of Oils, Fats and Derivatives*, 7th ed.; Blackwell Scientific Publications: Oxford, U.K., 1992.
(34) Leung, H. K.; Anderson, G. R.; Norr, P. J. Rapid Determination of Total and Solid Fat Contents in Chocolate Products by Pulsed Nuclear Magnetic Resonance. *J. Food Sci.* **1985**, *50* (4), 942−945.
(35) Rutledge, D. N.; Diris, J.; Bugner, E.; Belliardo, J.-J. Biological Reference Materials for the Verification of Sample Preparation and Measurement by Low Resolution NMR. *Fresenius J. Anal. Chem.* **1990**, *338* (4), 441−448.

https://doi.org/10.1021/acs.energyfuels.2c03309
Energy Fuels 2023, 37, 291−300